Research Article

Proteins: Structure, Function and Bioinformatics
DOI 10.1002/prot.25455

Crystal structure of tetrameric human Rabin8 GEF domain

Short title: *Crystal structure of tetrameric Rabin8*

Melanie Vetter[1], Niels Boegholm[2], Anni Christensen[2], Sagar Bhogaraju[1], Marie B. Andersen[2], Anna Lorentzen[2] and Esben Lorentzen[2*]

[1] Max-Planck-Institute of Biochemistry, Department of Structural Cell Biology, Am Klopferspitz 18, D-82152 Martinsried, Germany

[2] Department of Molecular Biology and Genetics, Aarhus University, Gustav Wieds Vej 10c, DK-8000Aarhus C, Denmark.

Short title: *Crystal structure of tetrameric Rabin8*

* Correspondence to: Assoc. Prof. Esben Lorentzen, Department of Molecular Biology and Genetics, Aarhus University, Gustav Wieds Vej 10c, DK-8000Aarhus C, Denmark, Tel: +45 871 55478, E-mail: el@mbg.au.dk

Keywords**:** cilium, Rabin8, Rab8, guanine nucleotide exchange, crystal structure, tetramer, ciliary targeting complexes

Received: Jul 28, 2017; Revised: Dec 24, 2017; Accepted: Jan 05, 2018

ABSTRACT

Rab GTPases and their effectors, activators and guanine nucleotide exchange factors (GEFs) are essential for vesicular transport. Rab8 and its GEF Rabin8 function in formation of the cilium organelle important for developmental signaling and sensory reception. Here we show by size exclusion chromatography and analytical ultracentrifugation that Rabin8 exists in equilibrium between dimers and tetramers. The crystal structure of tetrameric Rabin8 GEF domain reveals an occluded Rab8 binding site suggesting that this oligomer is enzymatically inactive, a notion we verify experimentally using Rabin8/Rab8 GEF assays. We outline a procedure for the purification of active dimeric Rabin8 GEF-domain for *in vitro* activity assays.

1. INTRODUCTION

Cilia are organelles that protrude from most eukaryotic cells and serve multiple important functions including motility, signaling and sensory reception. Ciliogenesis relies on the action of several macro-molecular complexes including ciliary targeting complexes [1,2], intraflagellar transport (IFT) complexes and complexes of Bardet-Biedl syndrome (BBS) proteins termed BBSome [3-5]. Transport of Golgi-derived vesicles to the basal-body region and fusion with the plasma membrane is required for cilium formation and delivery of cilium-specific membrane proteins [6-10]. Rab GTPases are important for membrane identity [11] and several Rabs including Rab8, Rab11 and Rab23, were shown to be required for the process of ciliogenesis and ciliary trafficking [5,10,12-15]. Vesicular transport to the cilium organelle relies on a number of additional factors including Arf4, FIP3, Rabin8, and ASAP1 that dynamically assemble ciliary targeting complexes [6,10,16]. Rab11

was shown to be involved in the transport of Golgi and recycling endosome-derived vesicles to the plasma membrane [1,17-21]. Rab11 has numerous effectors including FIP3 and Rabin8 that simultaneously associate with the GTP-bound activated state of Rab11 (Fig. 1a-b) [2,7,22]. While FIP3 binds to the canonical effector binding site on Rab11, Rabin8 binds at an unusual effector-binding site, which allows for the simultaneous binding of FIP3 and Rabin8 to Rab11-GTP [22]. Rabin8 contains, in addition to the C-terminal Rab11-binding domain, a central coiled-coil domain that dimerizes and functions as a guanine nucleotide exchange factor (GEF) to activate Rab8 (Fig. 1a-b) [15,23]. Rab8 is required for the fusion of vesicles at the ciliary base as Rab8 inhibition leads to accumulation of rhodopsin carrying vesicles in photoreceptor cells [5,8,15]. Interestingly, Rab8 was also recently shown to be required for the delivery of recycling receptors to the immune synapse of T-cells [24].

Several studies demonstrated that Rabin8 binds Rab8 to stimulate the release of GDP [15,22,23]. Recently, it was shown that the Parkinson's disease kinase LRRK2 phosphorylates a number of Rab GTPases including Rab8 [25,26]. Phosphorylation of Rab8 T72 by LRRK2 regulates Rabin8 binding and results in a 4-fold reduction of Rabin8 GEF activity towards Rab8 [25]. The crystal structure of the Rabin8:Rab8 complex revealed that two copies of the central Rabin8 GEF domain homo-dimerizes to bind one copy of Rab8 [23]. This architecture is consistent with the fact that the C-terminal domain of Rabin8 also homo-dimerizes [22].

Some controversy exists with respect to the ability of Rab11 to stimulate the GEF activity of Rabin8 towards Rab8. While one previous study showed that the presence of Rab11 results in an increase in Rabin8 GEF activity towards Rab8 [15], another study did not

observe such a Rab11-mediated activation [22]. Here we demonstrate that Rabin8 exists in equilibrium between active dimers and inactive tetramers. The crystal structure of tetrameric Rabin8 provides a molecular basis for the reduced GEF activity as the Rab8-binding site overlaps with the tetramerization interface. Our data suggest that Rabin8 activity is dependent on the oligomeric state and particular care should be given to purification strategy to obtain reproducible *in vitro* GEF assay results.

2. MATERIALS AND METHODS

2.1 Purification of Rabin8 protein constructs

Human full length Rabin8 ($Rabin8_{FL}$), $Rabin8_{144-C}$, $Rabin8_{144-245}$ (the Rabin8 GEF domain, see Fig. 1a) or $Rabin8_{171-245}$ were over-expressed from pEC vectors with N-terminal tobacco etch virus (TEV) cleavable hexa-histidine tags. 6-9 L of *E.coli* BL21 (DE3), grown in terrific broth medium, were induced with 0.5 mM IPTG overnight at 18 °C. Cells were lysed by sonication in lysis buffer (50 mM phosphate pH 7.5, 150 mM NaCl, 10% glycerol, 5 mM $MgCl_2$ and 5 mM beta-mercaptoethanol. Purification was carried out by loading the lysate onto a 5 mL HisTrap HP column (GE healthcare), which was equilibrated in lysis buffer supplemented with 10 mM imidazole. Subsequently the column was washed with 5-10 column volumes (CVs) of lysis buffer with the addition of 1 M NaCl. To remove heat shock protein contaminants at least 10-15 CVs of heat shot protein removal buffer (50 mM Tris pH 7.5, 50 mM KCl, 10 mM $MnCl_2$ and 2 mM ATP) was applied to the Ni^{2+} column, followed by a final 1-2 CVs wash with lysis buffer. Bound proteins were eluted with a gradient of 10-500 mM imidazole (added to the lysis buffer). The elution peak containing Rabin8 protein was combined and dialyzed

overnight at 4 °C in buffer A (20 mM Tris pH 7.5, 50 mM NaCl, 5 mM $MgCl_2$ and 1 mM DTT) with the addition of 1 mg of TEV protease to cleave the His-tag.

The Rabin8 protein was then loaded onto a Q-sepharose ion exchange chromatography column and eluted with a 50-1000 mM NaCl gradient. Eluted Rabin8 protein was pooled, concentrated to 5-8 mg/ml and spun for 10 min at 15.000 g in a tabletop centrifuge to remove any precipitation before loading 200 µL onto a 10/300 GL Superdex200 (GE healthcare) gelfiltration column. Although $Rabin8_{GEF}$ is only 11 kDa in size, the molecule is highly elongated, and we thus recommend the Superdex200 rather then a Superdex75 column to achieve the necessary resolution to separate dimers from tetramers. If the dimer and tetramer peaks are not well separated on the Superdex200 column, we recommend cleaning the column with 1 CV of 0.5 M NaOH followed by re-equilibration before usage. Rabin8 protein constructs were eluted during the final SEC purification step in a buffer containing 10 mM Hepes pH 7.5, 150 mM NaCl, 2 mM DTT and 5 mM $MgCl_2$. Fractions corresponding to dimers and tetramers were kept separate and overlap regions between the two peaks were avoided when combining samples for GEF assays. Concentrations were measured for all fractions and relevant fractions combined to achieve the necessary concentration for GEF assays and pull-downs experiments (concentrating the protein at this stage should be avoided). The $Rabin8_{GEF}$ protein construct does not contain a tryptophan and it is thus important to take the relatively low extinction coefficient of 0.127 into account when assessing the protein concentration.

2.2 Crystallization, data collection and refinement of the tetrameric Rabin8 structure

Crystals of tetrameric Rabin8 GEF domain were obtained by mixing protein in SEC buffer (see above) at a concentration of 10 mg/ml with a precipitant solution containing 50 mM Tris pH 7.3 and 40% MPD in sitting drop vapour diffusion experiments using 96-well polystyrene Greiner plates. Crystals appeared after 4 days at 18 °C and, as the crystallization condition also constituted a cryo protection condition, could be directly cooled in liquid nitrogen. X-ray diffraction data were collected from native crystals at the Swiss Light Source and processed to 2.45Å resolution with XDS [27] (see Table I). The native Patterson function showed a large none origin peak (36% of origin peak height), indicative of translational pseudo symmetry (likelihood of not having translational pseudo symmetry is $5.5*10^{-4}$ according to the Phenix Xtriage program [28]). Phases for the structure factors were obtained by soaking crystals in mother liquor containing 1 mM AuCN overnight and flash cooled in liquid nitrogen before collecting single anomalous dispersion data to 2.75Å resolution. The anomalous signal extended to 3.4Å resolution and was used in Phenix autosol [28] to locate 4 gold ions and calculate initial phases with a figure of merit of 0.324 for the entire 45-2.75Å resolution range. Density modification with 56% solvent content and four fold NCS averaging was carried out as part of the autosolve procedure in Phenix, which produced an initial electron density map into which $Rabin8_{GEF}$ helices were placed (Fig. S3). An initial model containing four $Rabin8_{GEF}$ monomers was built in the experimental map using Coot [29] and the structure refined against the native data in Phenix refine [28] using NCS torsion angle restraints, secondary structure restraints and four groups for each Rabin8 chain in TLS refinement but without

real space refinement. Waters were placed manually into spherical densities with plausible hydrogen-bonding networks. The structure was completed by iterative cycles of building and refinement against the native data.

2.3 Analytical ultracentrifugation

Sedimentation velocity data were collected using an Optima XL-I analytical ultracentrifuge (Beckman) equipped with an An-60 Ti rotor and double-sector epon centerpieces. Full length and truncated Rabin8 was buffered with 10 mM HEPES, pH 7.5, 150 mM NaCl, 5 mM $MgCl_2$, and 2 mM TCEP at concentrations of 0.4 or 4 mg/ml. Buffer densities and viscosities were determined with a DMA 5000 densitometer and an AMVn viscosimeter (Anton Paar). Protein concentration distribution at room temperature was monitored at 280 nm at 235.000 g. Time-derivative analysis was computed with the SEDFIT package, version 12.1b [30], to determine a c(s) distribution and estimate molecular weights Mf.

2.4 GST-Rab8 pulldown of Rabin8

200 µl of 10 µM GST-tagged human Rab8 protein was immobilised on 20 µl of GSH-affinity resin using a binding buffer containing 20 mM TrisHCl pH 7.5, 150 mM NaCl, 5 mM $MgCl_2$, 5% glycerol and 2 mM DTT and incubated for 2h at 4 °C on a rotating wheel. The resin was collected by centrifugation (500 g, 4 °C), and washed one time with binding buffer. 200 µl of 20 µM WT or mutant dimeric $Rabin8_{GEF}$ was added to the beads followed by incubation for 2h at 4 °C on a rotating wheel and 3x washing with 1 mL of

binding buffer. Bound protein was eluted with 40 µl of binding buffer containing 20 µM reduced glutathione and analysed by SDS-PAGE.

2.5 Nucleotide exchange assays

GEF assays were always carried out with freshly purified $Rabin8_{GEF}$ by combining fractions from dimer or tetramer peaks as soon as they eluted from the SEC column without concentration of the sample. To measure Rabin8 GEF activity towards Rab8, nucleotide free $Rab8a_{1–183}$ was incubated with a 1.5-fold molar excess of 2′(3′)-*O*-(*N*-methylanthraniloyl)-GDP (mant-GDP, Jena Bioscience) for 2 h at room temperature. The excess of mant-GDP was removed by a Micro Bio-Spin column (BioRad). 1 µM mant-GDP–bound Rab8 was incubated for 30 min at 20 °C with 3 µM purified $Rabin8_{GEF}$ in a buffer containing 30 mM Tris, pH 7.5, 5 mM $MgCl_2$, 3 mM DTT and 10 mM potassium phosphate, pH 7.4 (total volume of 50 µL for experiments shown in Figs. 4 and 6; 300 µL for the experiments in Fig. 5). The nucleotide-exchange reaction was initiated by addition of 1 mM GTP. The dissociation of mant-GDP from Rab8 was measured in a quartz Hellman cuvette without stirring using a fluorescence spectrometer from PerkinElmer (Figs. 4 and 6, monochrometer slit width of 5 mm) or Photon Technology International (Fig. 5, monochrometer slit with of 4 mm) with 366 nm excitation and 450 nm emission at 20 °C. Fluorescence emission was read out every 2 s for a total of 300 s for the experiments shown in Figs. 4 and 6 or every 1 s for a total of 600 s for the experiments shown in Fig. 5. The relative fluorescence data were fitted to a one-phase exponential-decay equation without constraints using nonlinear regression and the resulting observed rate constants (kobs) were calculated with Prism 6.0. The quantifications of Rabin8 GEF

activity shown in Figs. 4b and 6c were calculated for three independent experiments (five independent experiments for 5c) and displayed as average values and standard deviations.

3. RESULTS

3.1 Rabin8 forms homo-dimers and homo-tetramers *in vitro*

During the purification of recombinantly expressed human Rabin8 GEF domain (Fig. 1a, residues 144-245, hereafter referred to as $Rabin8_{GEF}$), we noticed that the protein reproducibly eluted from size exclusion chromatography (SEC) in two distinct peaks suggestive of different oligomeric states (Fig. 1c). When analyzed by SDS-PAGE, both SEC peaks were shown to contain the ~11 kDa $Rabin8_{GEF}$ domain (Fig. 1d). Over-night storage of separately combined $Rabin8_{GEF}$ SEC peaks resulted in the reappearance of a double peak demonstrating interconvertibility of the two forms (Fig. S1). $Rabin8_{GEF}$ is known to bind Rab8 in a trimeric complex containing a homo-dimer of $Rabin8_{GEF}$ and one subunit of Rab8 [23]. Consistent with this notion, we found that a complex of $Rabin8_{GEF}$ incubated over-night with excess $Rab8_{1-183}$(T22N) eluted in SEC as a single peak located between the two peaks of $Rabin8_{GEF}$ (Fig. 1c). This result demonstrated that the presence of Rab8 prevents the formation of the higher molecular weight (Mw) oligomeric state of $Rabin8_{GEF}$.

Next, we characterized the two Rabin8 states using the complementary method of velocity sedimentation analytical ultracentrifugation (AUC), which provides quantitative data of better resolution than SEC. Consistent with a 2:1 architecture of the Rabin8-Rab8 complex, we observed a Mw of 42kDa for the $Rabin8_{GEF}$:Rab8 complex (Fig. 1e and S2a). As $Rabin8_{GEF}$ does not contain a tryptophan residue, we could not detect this

construct by AUC. However, a longer construct of Rabin8$_{144\text{-}C}$ containing both the GEF and the C-terminal domains was subjected to AUC (Fig. S2b). Measured sedimentation coefficients are consistent with a mixture of Rabin8$_{144\text{-}C}$ homo-dimers and homo-tetramers (Fig. 1e and S2b). Rabin8$_{FL}$ also displayed a sedimentation coefficient distribution consistent with both dimers and tetramers in AUC (Fig. 1e and S2c). As the C-terminal Rabin8 domain alone (without the presence of the GEF domain) was previously shown to form a homo-dimer by AUC [22], we conclude that the central GEF domain of Rabin8 is responsible for the observed dimer-tetramer equilibrium.

3.2 Rabin8$_{GEF}$ tetramer crystal structure

To elucidate the molecular basis of Rabin8 tetramerization, purified Rabin8$_{GEF}$ was crystallized and the structure determined at 2.45Å resolution. Molecular replacement with monomeric or dimeric Rabin8$_{GEF}$ from the previously determined Rabin8-Rab8 structure [23] (pdb code 4LHX) failed, possibly due to conformational changes and the presence of translational non-crystallographic symmetry. Consequently, we determined the structure of Rabin8$_{GEF}$ experimentally from single anomalous dispersion data collected on a gold derivative. Experimentally derived electron density clearly revealed the presence of four interacting helices suggesting a tetrameric structure (Fig. S3). Four Rabin8$_{GEF}$ molecules, each consisting of one long ~100 residue α-helix, were built into the electron density of the asymmetric unit and refined against native X-ray diffraction data to yield a model with good geometry and an R_{free} of 30.5% (see Table I). The relatively high R_{free} is likely a result of strong translational non-crystallographic symmetry.

The crystal structure revealed that the Rabin8$_{GEF}$ tetramer forms an elongated complex with overall dimensions of 200x30x20 Å^3 (Fig. 2). In the Rabin8$_{GEF}$ tetramer, two parallel dimers interact in an anti-parallel fashion (Fig. 2a). This tetramerization mode requires partial opening of the Rabin8$_{GEF}$ dimers, where the ~50 most N-terminal residues of one Rabin8$_{GEF}$ dimer unzips to engage in contacts with a second unzipped Rabin8$_{GEF}$ dimer. This results in a large conformational change of the N-terminal part of the Rabin8$_{GEF}$ tetramer when compared to the dimeric Rabin8$_{GEF}$ as shown in Fig. 2b. Whereas the C-terminal parts of tetrameric and dimeric Rabin8$_{GEF}$ superpose well (0.5 Å rmsd between C-alpha atoms of residues 205-225), the N-terminal parts (residues 157-190) deviate significantly in conformation (more than 10Å from residue 157 in dimeric and tetrameric Rabin8, see Fig. 2b). Residues that interact to form the N-terminal coiled-coil domain of dimeric Rabin8$_{GEF}$ are positioned too far from each other to interact directly in the tetramer. Instead, these residues engage in interactions with residues of the neighboring dimer thus participating in tetramerization (Fig. 2b). Each Rabin8$_{GEF}$ monomer interacts with the other three monomers mainly via hydrophobic interactions (Fig. 2c), burying a total surface area of ~2750Å^2 per monomer. The dimer/tetramer equilibrium of Rabin8 is thus likely mediated by zipping/unzipping of the N-terminal region of the coiled-coil GEF domain. The fully zipped Rabin8 adopts a dimeric structure whereas one partially unzipped Rabin8 dimer interacts with a second partially unzipped Rabin8 dimer to form a tetramer.

3.4 GEF activity towards Rab8 is strongly reduced for tetrameric Rabin8$_{GEF}$

Rabin8 mediates the nucleotide exchange (GDP to GTP) of Rab8 through recruitment of Rab8 to the central part of the Rabin8 GEF domain (residues ~189-207, ref. [23]). Interestingly, in the tetrameric Rabin8 GEF domain structure presented here, the two potential Rab8 binding sites are effectively occluded (Fig. 3a). In the tetrameric Rabin8$_{GEF}$ structure, the Rab8 binding site is occupied by the N-terminal 20 amino acids (residues 150-170) of the neighboring Rabin8$_{GEF}$ dimer (Fig. 3a). Most of the Rab8-interacting residues instead interact with the second Rabin8$_{GEF}$ dimer in tetrameric Rabin8 (Fig. 3b-c). The structural analysis presented in Fig. 3 thus suggests that tetrameric Rabin8 is inactive as a GEF towards Rab8 because of steric reasons. To test this notion experimentally, we prepared dimeric or tetrameric Rabin8$_{GEF}$ by SEC (Fig. 1c) and immediately carried out GEF assays where the exchange of fluorescently labeled Mant-GDP by GTP was followed over time (Fig. 4). The Rabin8$_{GEF}$ dimer showed robust GEF activity 13X higher than the intrinsic GDP exchange (Fig. 4). In comparison, the GEF activity of tetrameric Rabin8$_{GEF}$ was only 3X higher than the intrinsic activity (Fig. 4). This result demonstrates that tetrameric Rabin8 is significantly less active as a GEF towards Rab8 than dimeric Rabin8. The fact that tetrameric Rabin8$_{GEF}$ GEF activity is higher than the intrinsic Rab8 exchange activity (Fig. 4) may be a result of interconverted dimeric Rabin8$_{GEF}$ formed during the ~1 h it takes to complete the SEC and GEF assays. Altogether, the data of Figures 3-4 support the notion that the Rabin8 tetramer has an occluded Rab8-binding site with significantly reduced GEF activity.

3.5 Residues 145-170 are required for Rabin8$_{GEF}$ tetramerization but not for GEF activity

The structural analysis of Rabin8$_{GEF}$ presented in Figures. 2-3 suggests that residues 150-170 of Rabin8 are required for tetramerization but not for Rab8 binding. To test this notion experimentally, a shorter Rabin8$_{171-245}$ construct was recombinantly expressed and purified (Fig. 5a). In agreement with the structural prediction, Rabin8$_{171-245}$ gave a single peak in SEC consistent with a dimeric state (compare Figures 1c and 5a). The absence of the second peak demonstrates that tetramerization is effectively abolished for this construct. Given that residues 190-210 of Rabin8 constitutes the Rab8-binding site, Rabin8$_{171-245}$ is predicted to retain full GEF activity towards Rab8. To test this notion experimentally we carried out GEF assays using the Rabin8$_{171-245}$ construct (Fig. 5b-c). The results show that Rabin8$_{171-245}$ increases the exchange rate of Rab8 GDP by 25X in comparison to the intrinsic rate (Fig. 5c). The fact that the measured exchange rate is higher than for dimeric Rabin8$_{GEF}$ (Fig. 4b) may reflect that Rabin8$_{171-245}$ is strictly dimeric and does not convert into inactive tetramers during the course of the GEF experiment. The crystal structure of tetrameric Rabin8 presented in Figs. 2-3 thus allows for structure-based predictions regarding activity and ologimeric state of Rabin8 constructs. Altogether, the data presented in Fig. 5 demonstrate that residues 145-170 of Rabin8 are required for tetramerization but not for GEF activity towards Rab8.

3.6 Mutational analysis of the Rab8 binding site of Rabin8

Although the Rabin8:Rab8 crystal structure is known [23], a comprehensive mutational study of Rab8-binding residues in Rabin8 has not ben carried out. To elucidate the

importance of Rabin8 residues involved in Rab8 association and nucleotide exchange, we mutated interface residues in $Rabin8_{GEF}$ to alanines and purified the variants (E192A, L196A, T197A, F201A or M207A, see Fig. 3b and 6a). All five tested point mutants of $Rabin8_{GEF}$ displayed dimer/tetramer equilibriums in SEC similar to the WT protein (data not shown), which demonstrated that none of the mutations abolished tetramer formation. This is consistent with the fact that tetramerization relies on residues 145-170 located N-terminally to the Rab8-bindsing site (Fig. 2b). To evaluate the impact of these mutations on GEF activity and Rab8-binding, the SEC peaks corresponding to dimeric $Rabin8_{GEF}$ mutants were pooled for each point mutant and used for pull-down and GEF activity assays (Fig. 6). L196 of Rabin8 makes hydrophobic interactions with F70 and Y77 of Rab8 and the $Rabin8_{GEF}$ L196A mutant had only marginally reduced affinity for Rab8 (Fig. 6a). GEF activity was also only marginally impaired and showed only a 15% reduction compared to WT Rabin8 (Fig. 6b-c). T197 of Rabin8 makes a hydrogen bond with Y77 of Rab8 and mutation to alanine reduced Rab8-binding slightly and GEF activity by ~30%. More severe is the M207A mutation that still bound Rab8 but had 3-4 fold reduced GEF activity compared to WT. M207 makes hydrophobic contacts with F37 of the switch I region of Rab8 and may be involved in the GDP release mechanism. Mutation of F201, that interacts with I43, F37 and W62 of Rab8, to alanine completely abolished Rab8 binding and reduced GDP exchange activity to intrinsic Rab8 levels. Similarly, E192, that interacts with switch II of Rab8, was absolutely required for Rab8-interaction and Rabin8 assisted GDP->GTP exchange (Fig. 6). The results from this mutational analysis of $Rabin8_{GEF}$ are in agreement with the Rab8:Rabin8 crystal structure previously published [23] and pinpoints residues important for Rabin8 GEF activity.

4. DISCUSSION

Here we demonstrate that Rabin8 exists in equilibrium between dimers and tetramers *in vitro*. The tetramerization of Rabin8 relies on the central coiled-coil GEF domain of which we determine the crystal structure to provide a molecular basis for tetramerization. Activity assays with dimeric and tetrameric Rabin8 GEF domains demonstrate that tetramerization of Rabin8 results in strongly reduced GEF activity towards Rab8 when compared to dimeric Rabin8 GEF activity. Our crystal structure suggests that the reason for the reduced activity is steric hindrance resulting in an occluded Rab8 binding site in tetrameric Rabin8. Based on the structural data, we designed a $Rabin8_{171\text{-}245}$ truncation where tetramerization residues were deleted. This construct is strictly dimeric and, as expected, has full GEF activity.

These findings have implications for the reproducibility of Rabin8 GEF assays where different results will be obtained depending on the ratio of dimer/tetramer of the Rabin8 preparation used. Rabin8 prepared without a SEC purification step or using a SEC column with insufficient resolution to separate the two oligomeric states will give lower apparent GEF activity than dimeric Rabin8 purified by SEC. Additionally, given that purified dimeric Rabin8 converts back into a dimer/tetramer mixture over time (Fig. S1), purified Rabin8 will display different GEF activities depending on time of storage. These observations may account for the different Rabin8 GEF activities reported in the literature. We thus recommend the procedure outlined in Materials & Methods to obtain reproducible results in Rabin8:Rab8 GEF assays.

References

1. Deretic D (2013) Crosstalk of Arf and Rab GTPases en route to cilia. smallgtpases 4:70–77.

2. Vetter M, Wang J, Lorentzen E, Deretic D (2015) Novel topography of the Rab11-effector interaction network within a ciliary membrane targeting complex. smallgtpases 6:165–173.

3. Taschner M, Lorentzen E (2016) The Intraflagellar Transport Machinery. Cold Spring Harbor Perspectives in Biology.

4. Follit JA, Li L, Vucica Y, Pazour GJ (2010) The cytoplasmic tail of fibrocystin contains a ciliary targeting sequence. The Journal of Cell Biology.

5. Nachury MV, Loktev AV, Zhang Q, Westlake CJ, Peränen J, Merdes A, Slusarski DC, Scheller RH, Bazan JF, Sheffield VC, et al. (2007) A core complex of BBS proteins cooperates with the GTPase Rab8 to promote ciliary membrane biogenesis. Cell 129:1201–1213.

6. Wang J, Morita Y, Mazelova J, Deretic D (2012) The Arf GAP ASAP1 provides a platform to regulate Arf4- and Rab11–Rab8-mediated ciliary receptor targeting. EMBO J 31:4057–4071.

7. Wang J, Deretic D (2015) The Arf and Rab11 effector FIP3 acts synergistically with ASAP1 to direct Rabin8 in ciliary receptor targeting. Journal of Cell Science 128:1375–1385.

8. Westlake CJ, Baye LM, Nachury MV, Wright KJ, Ervin KE, Phu L, Chalouni C, Beck JS, Kirkpatrick DS, Slusarski DC, et al. (2011) Primary cilia membrane assembly is initiated by Rab11 and transport protein particle II (TRAPPII) complex-dependent trafficking of Rabin8 to the centrosome. Proc Natl Acad Sci U S A 108:2759–2764.

9. Lu Q, Insinna C, Ott C, Stauffer J, Pintado PA, Rahajeng J, Baxa U, Walia V, Cuenca A, Hwang Y-S, et al. (2015) Early steps in primary cilium assembly require EHD1/EHD3-dependent ciliary vesicle formation. Nature Cell Biology 17:228–240.

10. Mazelova J, Astuto-Gribble L, Inoue H, Tam BM, Schonteich E, Prekeris R, Moritz OL, Randazzo PA, Deretic D (2009) Ciliary targeting motif VxPx directs assembly of a trafficking module through Arf4. EMBO J 28:183–192.

11. Barr FA (2013) Review series: Rab GTPases and membrane identity: causal or inconsequential? The Journal of Cell Biology 202:191–199.

12. Zhen Y, Stenmark H (2015) Cellular functions of Rab GTPases at a glance. Journal of Cell Science 128:3171–3176.

13. Boehlke C, Bashkurov M, Buescher A, Krick T, John AK, Nitschke R, Walz G,

Kuehn EW (2010) Differential role of Rab proteins in ciliary trafficking: Rab23 regulates Smoothened levels. Journal of Cell Science 123:1460–1467.

14. Lim YS, Chua CEL, Tang BL (2011) Rabs and other small GTPases in ciliary transport. Biol. Cell 103:209–221.

15. Knödler A, Feng S, Zhang J, Zhang X, Das A, Peränen J, Guo W (2010) Coordination of Rab8 and Rab11 in primary ciliogenesis. Proc Natl Acad Sci U S A 107:6346–6351.

16. Sung C-H, Leroux MR (2013) The roles of evolutionarily conserved functional modules in cilia-related trafficking. Nature Cell Biology 15:1387–1397.

17. Ullrich O (1996) Rab11 regulates recycling through the pericentriolar recycling endosome. J. Cell Biol. 135:913–924.

18. Chen W, Feng Y, Chen D, Wandinger-Ness A (1998) Rab11 Is Required for Trans-Golgi Network–to–Plasma Membrane Transport and a Preferential Target for GDP Dissociation Inhibitor. Mol Biol Cell 9:3241–3257.

19. Ren M, Xu G, Zeng J, De Lemos-Chiarandini C, Adesnik M, Sabatini DD (1998) Hydrolysis of GTP on rab11 is required for the direct delivery of transferrin from the pericentriolar recycling compartment to the cell surface but not from sorting endosomes. Proc Natl Acad Sci U S A 95:6187–6192.

20. Skop AR, Bergmann D, Mohler WA, White JG (2001) Completion of cytokinesis in C. elegans requires a brefeldin A-sensitive membrane accumulation at the cleavage furrow apex. Current Biology 11:735–746.

21. Pellinen T (2006) Integrin traffic. Journal of Cell Science 119:3723–3731.

22. Vetter M, Stehle R, Basquin C, Lorentzen E (2015) Structure of Rab11–FIP3–Rabin8 reveals simultaneous binding of FIP3 and Rabin8 effectors to Rab11. Nat Struct Mol Biol 22:695–702.

23. Guo Z, Hou X, Goody RS, Itzen A (2013) Intermediates in the Guanine Nucleotide Exchange Reaction of Rab8 Protein Catalyzed by Guanine Nucleotide Exchange Factors Rabin8 and GRAB. Journal of Biological Chemistry 228:32466–32474.

24. Finetti F, Patrussi L, Galgano D, Cassioli C, Perinetti G, Pazour GJ, Baldari CT (2015) The small GTPase Rab8 interacts with VAMP-3 to regulate the delivery of recycling T-cell receptors to the immune synapse. Journal of Cell Science 128:2541–2552.

25. Steger M, Tonelli F, Ito G, Davies P, Trost M, Vetter M, Wachter S, Lorentzen E, Duddy G, Wilson S, et al. (2016) Phosphoproteomics reveals that Parkinson's disease kinase LRRK2 regulates a subset of Rab GTPases. Elife 5:e12813.

26. Steger M, Diez F, Dhekne HS, Lis P, Nirujogi RS, Karayel O, Tonelli F, Martinez TN, Lorentzen E, Pfeffer SR, et al. (2017) Systematic proteomic analysis of LRRK2-mediated Rab GTPase phosphorylation establishes a connection to ciliogenesis. Elife 6.

27. Kabsch W (2010) XDS. Acta Crystallogr D Biol Crystallogr 66:125–132.

28. Adams PD, Afonine PV, Bunkóczi G, Chen VB, Davis IW, Echols N, Headd JJ, Hung L-W, Kapral GJ, Grosse-Kunstleve RW, et al. (2010) PHENIX: a comprehensive Python-based system for macromolecular structure solution. Acta Crystallogr D Biol Crystallogr 66:213–221.

29. Emsley P, Cowtan K (2004) Coot: model-building tools for molecular graphics. Acta Crystallogr D Biol Crystallogr 60:2126–2132.

30. Schuck P (2000) Size-Distribution Analysis of Macromolecules by Sedimentation Velocity Ultracentrifugation and Lamm Equation Modeling. Biophys J.

Acknowledgements

We thank the staff at the Swiss light source for assistance with X-ray diffraction data collection, and the crystallization facility at the Max Planck Institute of Biochemistry for access to crystallization screening. We are also grateful to Dr. Stefan Uebel from the microchemistry Core Facility at the Max Planck Institute for analyzing proteins by analytical ultracentrifugation. We thank the Novo Nordisk Foundation (grant no. NNF15OC0014164) for funding. Structural coordinates have been deposited at PDB with the accession code 6F6P.

Figure legends

Fig.1: **a,** domain architecture of human Rabin8 with GEF and C-terminal Rab11 binding domains is indicated. **b,** Schematic representation of the interaction network of dimeric Rabin8 with different proteins shown in different colors. **c,** SEC elution profile of $Rabin8_{GEF}$ (blue line) and the $Rabin8_{GEF}$-$Rab8_{1-183}$(T22N) complex (purple). **d,**

Coomassie stained SDS-PAGE gel of the fractions from **c** indicated with the dashed lines. **e,** Table showing results from sedimentation velocity ultracentrifugation experiments (see also Fig. S2). Calculated and experimentally determined Mw values for various Rabin8 constructs and complexes are tabulated.

Fig. 2: **a,** Cartoon representation of the $Rabin8_{GEF}$ tetrameric structure in two perpendicular representations. Each of the two dimers forming the tetramer is shown in different colors. **b,** Cartoon representation of dimeric (grey) and tetrameric (cyan and magenta) $Rabin8_{GEF}$ after superpositioning the C-terminal residues of the molecules (residues 205-225). N–terminal residues that deviate by more than 10Å in the two structures are shown as sticks and labeled. **c,** Zoom in on the tetramerization interface reveals that mainly hydrophobic interactions hold the complex together.

Fig. 3: **a,** Cartoon representation of tetrameric Rabin8 and Rab8-Rabin8 complex structures after superpositioning. The position of Rab8 in the Rab8-Rabin8 structure clashes with the Rabin8 helix of the neighboring Rabin8 dimer making Rab8 binding mutually exclusive with Rabin8 tetramer formation. **b,** Zoom in on the Rab8 binding site on Rabin8 with interacting residues shown as sticks. **c,** Zoom in on the Rabin8 tetramer region representing the Rab8 binding site shown in panel **b**. The Rab8-interacting residues of Rabin8 are engaged in interactions with the neighboring dimer in the tetrameric Rabin8 structure.

Fig. 4: **a,** Rab8 GEF assay following the exchange of mant-GDP by GTP over time. Rab8 with the addition of buffer only (purple line, intrinsic Rab8 exchange activity), dimeric $Rabin8_{GEF}$ (blue line) or tetrameric $Rabin8_{GEF}$ (orange line) were used in the GEF assay. **b,** Quantification of the exchange rate for the GEF assay shown in panel **a**. Error bars represent standard deviation from 3 independent experiments.

Fig 5: **a,** SEC elution profile of $Rabin8_{171-245}$ (top) and Coomassie stained SDS-PAGE gel of peak fractions (bottom). The same SEC column was used as for Fig. 1c and the elution profiles are thus directly comparable. **b,** Rab8 GEF assay following the exchange of mant-GTP by GTP. Intrinsic exchange (purple line) or the $Rabin8_{171-245}$ catalyzed exchange $Rabin8_{171-245}$ (blue line) were assayed. The experiments were carried out using a different experimental setup compared to Figs. 4 and 6 as detailed in the materials and methods section. **c,** Quantification of the exchange rate for the GEF assay shown in panel **b**. Error bars represent standard deviation from 5 independent experiments.

Fig. 6: **a,** GST-tagged Rab8 was used to pull down WT or single point mutant variants of $Rabin8_{GEF}$. Proteins are visualized on a coomassie stained SDS-PAGE gel. **b,** Rab8 GEF assay using WT or point-mutant variants of $Rabin8_{GEF}$. Each point mutant is represented by a unique color. **c,** Quantification of the GEF assay shown in panel **b**. Error bars represent standard deviation from 3 independent experiments.

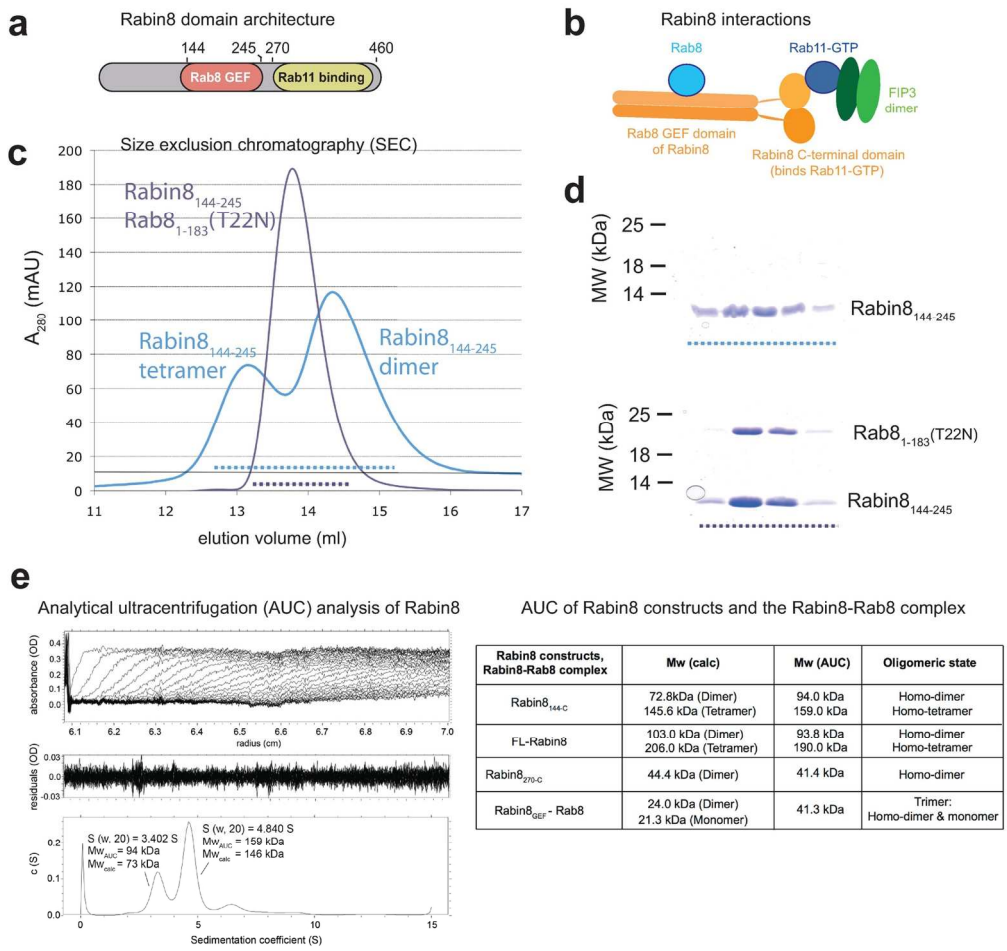

AUC of Rabin8 constructs and the Rabin8-Rab8 complex

Rabin8 constructs, Rabin8-Rab8 complex	Mw (calc)	Mw (AUC)	Oligomeric state
$Rabin8_{144-C}$	72.8kDa (Dimer) 145.6 kDa (Tetramer)	94.0 kDa 159.0 kDa	Homo-dimer Homo-tetramer
FL-Rabin8	103.0 kDa (Dimer) 206.0 kDa (Tetramer)	93.8 kDa 190.0 kDa	Homo-dimer Homo-tetramer
$Rabin8_{270-C}$	44.4 kDa (Dimer)	41.4 kDa	Homo-dimer
$Rabin8_{GEF}$ - Rab8	24.0 kDa (Dimer) 21.3 kDa (Monomer)	41.3 kDa	Trimer: Homo-dimer & monomer

Fig.1: a, domain architecture of human Rabin8 with GEF and C-terminal Rab11 binding domains is indicated. b, Schematic representation of the interaction network of dimeric Rabin8 with different proteins shown in different colors. c, SEC elution profile of Rabin8GEF (blue line) and the Rabin8GEF-Rab81-183(T22N) complex (purple). d, Coomassie stained SDS-PAGE gel of the fractions from c indicated with the dashed lines. e, Table showing results from sedimentation velocity ultracentrifugation experiments (see also Fig. S2). Calculated and experimentally determined Mw values for various Rabin8 constructs and complexes are tabulated.

151x142mm (300 x 300 DPI)

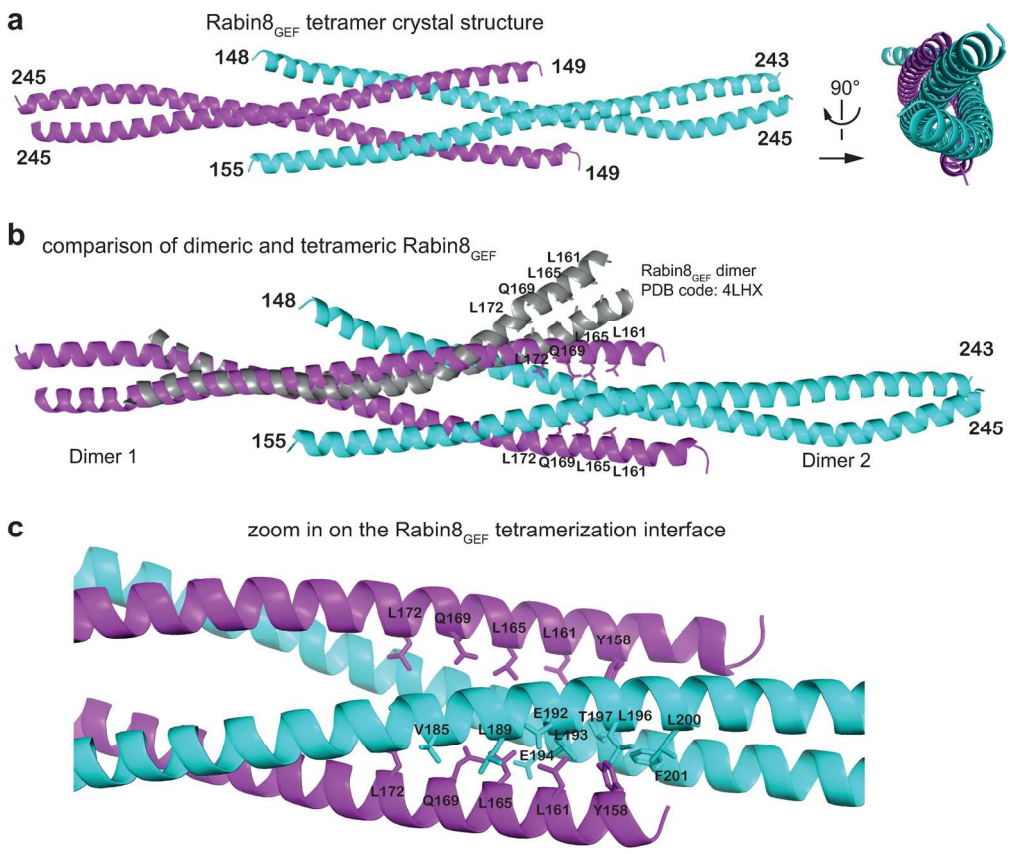

Fig. 2: a, Cartoon representation of the Rabin8GEF tetrameric structure in two perpendicular representations. Each of the two dimers forming the tetramer is shown in different colors. b, Cartoon representation of dimeric (grey) and tetrameric (cyan and magenta) Rabin8GEF after superpositioning the C-terminal residues of the molecules (residues 205-225). N–terminal residues that deviate by more than 10Å in the two structures are shown as sticks and labeled. c, Zoom in on the tetramerization interface reveals that mainly hydrophobic interactions hold the complex together.

166x140mm (300 x 300 DPI)

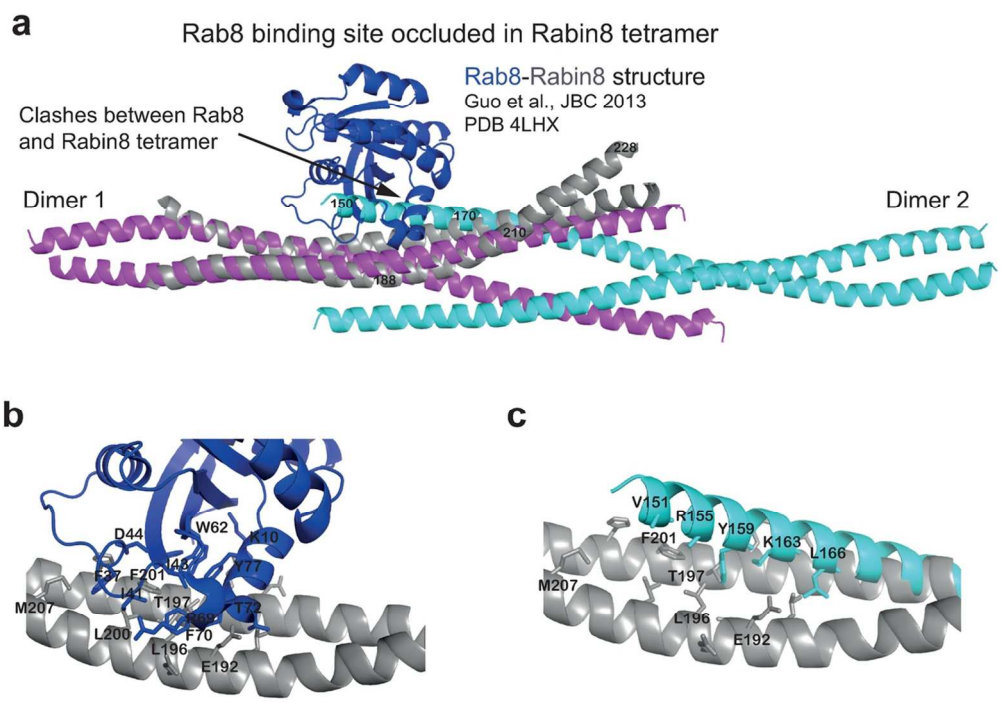

Fig. 3: a, Cartoon representation of tetrameric Rabin8 and Rab8-Rabin8 complex structures after superpositioning. The position of Rab8 in the Rab8-Rabin8 structure clashes with the Rabin8 helix of the neighboring Rabin8 dimer making Rab8 binding mutually exclusive with Rabin8 tetramer formation. b, Zoom in on the Rab8 binding site on Rabin8 with interacting residues shown as sticks. c, Zoom in on the Rabin8 tetramer region representing the Rab8 binding site shown in panel b. The Rab8-interacting residues of Rabin8 are engaged in interactions with the neighboring dimer in the tetrameric Rabin8 structure.

114x81mm (300 x 300 DPI)

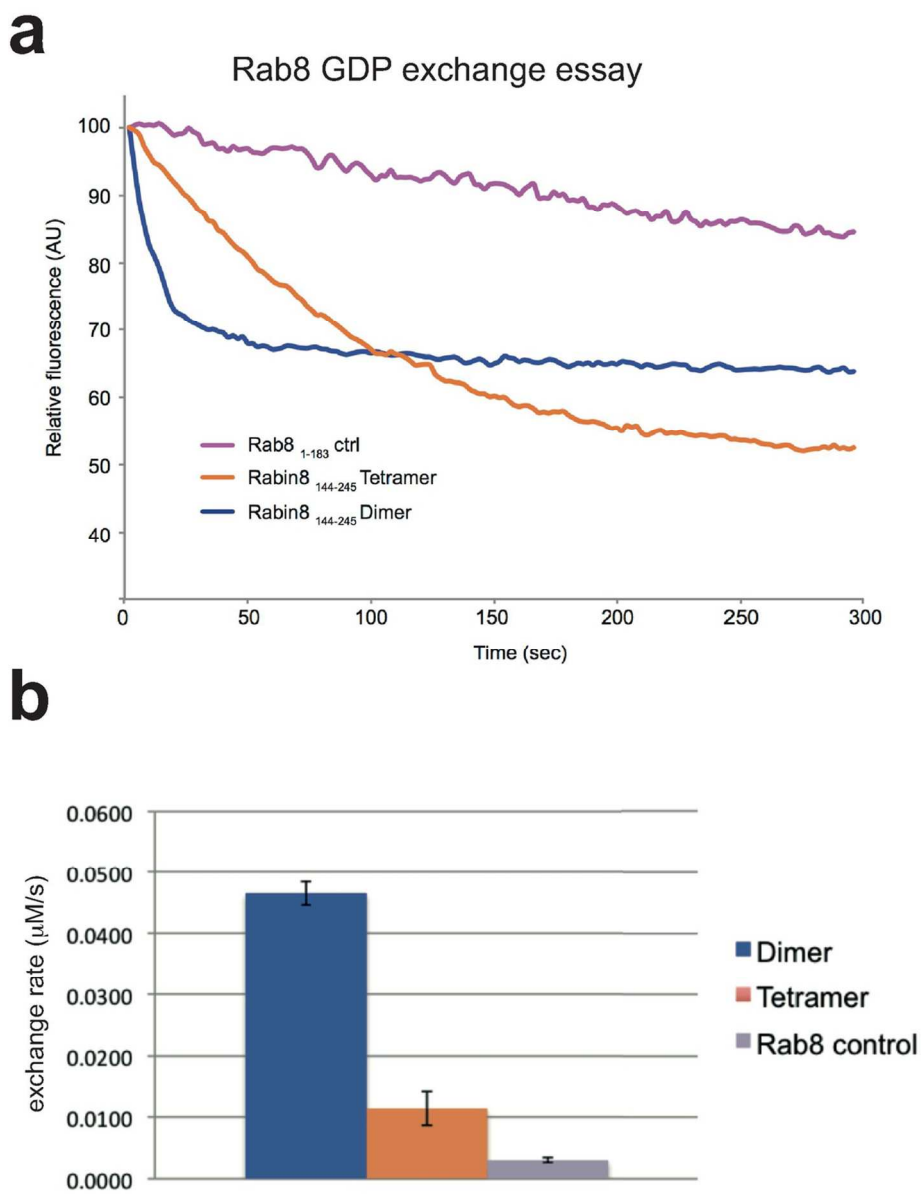

Fig. 4: a, Rab8 GEF assay following the exchange of mant-GDP by GTP over time. Rab8 with the addition of buffer only (purple line, intrinsic Rab8 exchange activity), dimeric Rabin8GEF (blue line) or tetrameric Rabin8GEF (orange line) were used in the GEF assay. b, Quantification of the exchange rate for the GEF assay shown in panel a. Error bars represent standard deviation from 3 independent experiments.

101x132mm (300 x 300 DPI)

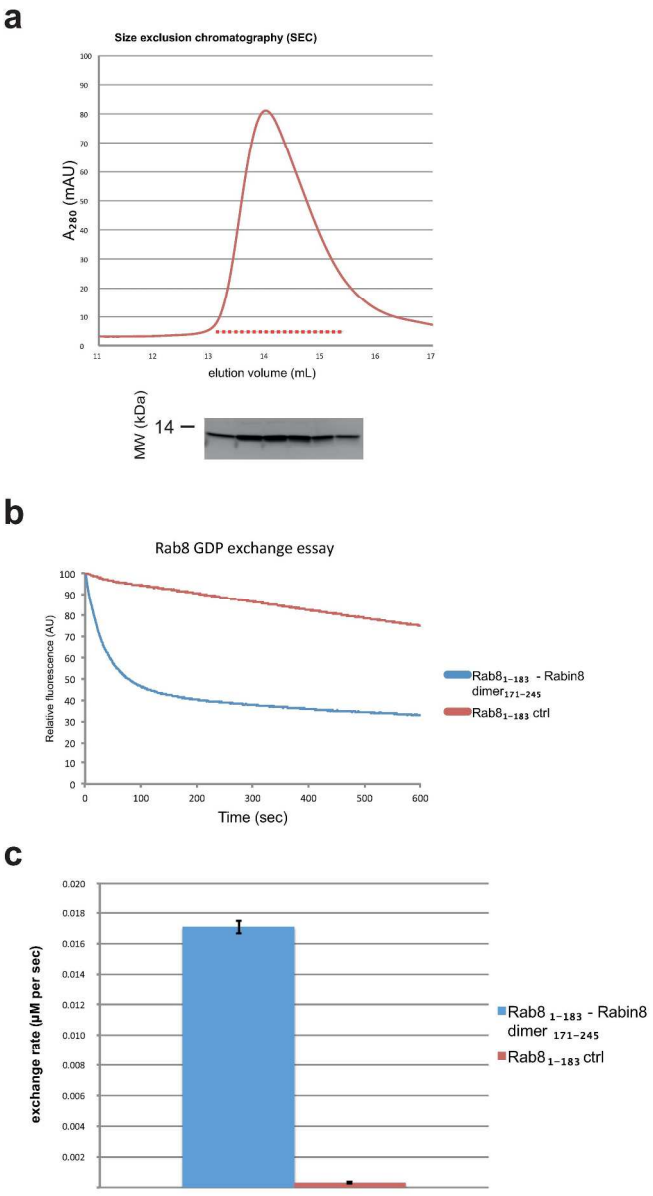

Fig 5: a, SEC elution profile of Rabin8171-245 (top) and Coomassie stained SDS-PAGE gel of peak fractions (bottom). The same SEC column was used as for Fig. 1b and the elution profiles are thus directly comparable. b, Rab8 GEF assay following the exchange of mant-GTP by GTP. Intrinsic exchange (purple line) or the Rabin8171-245 catalyzed exchange Rabin8171-245 (blue line) were assayed. The experiments were carried out using a different experimental setup compared to Figs. 4 and 6 as detailed in the materials and methods section. c, Quantification of the exchange rate for the GEF assay shown in panel b. Error bars represent standard deviation from 5 independent experiments.

208x373mm (300 x 300 DPI)

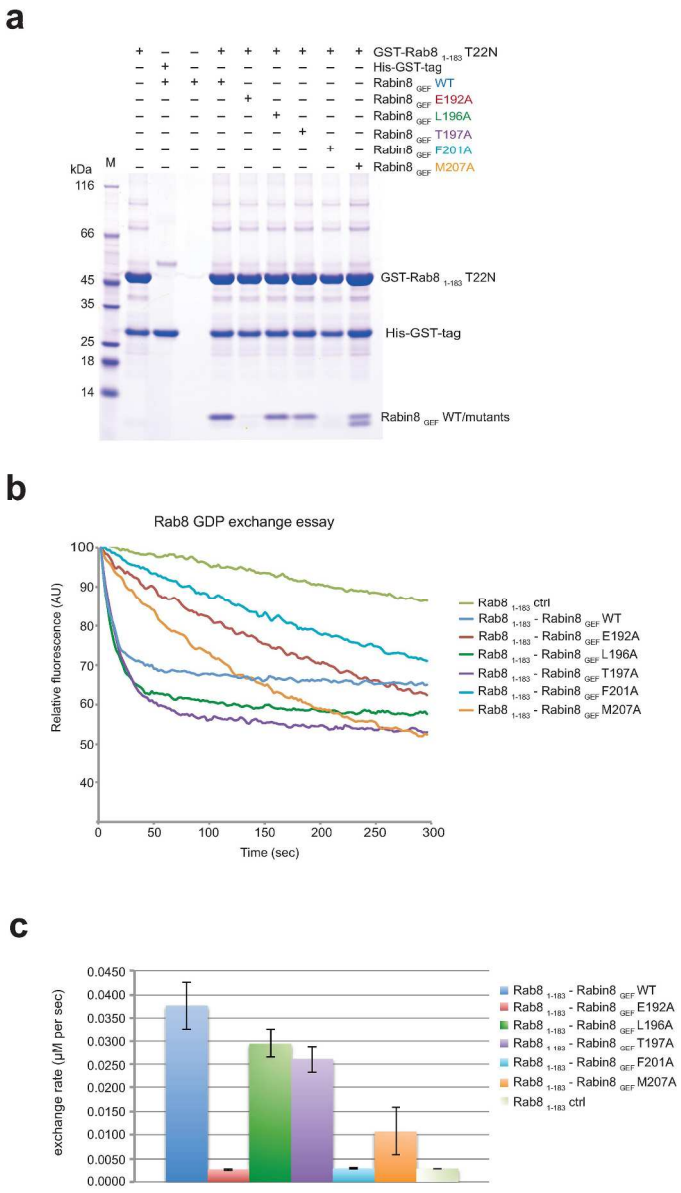

Fig. 6: a, GST-tagged Rab8 was used to pull down WT or single point mutant variants of Rabin8GEF. Proteins are visualized on a coomassie stained SDS-PAGE gel. b, Rab8 GEF assay using WT or point-mutant variants of Rabin8GEF. Each point mutant is represented by a unique color. c, Quantification of the GEF assay shown in panel b. Error bars represent standard deviation from 3 independent experiments.

202x362mm (300 x 300 DPI)

Table I. Data collection and refinement statistics.

Rabin8_GEF	Native data (PDB: 6F6P)	SAD data (AuCN soak)
Wavelength (Å)	1.0000	1.0376
Resolution range (Å)	68.6-2.45 (2.49- 2.45)	45-2.75 (2.91-2.75)
Space group	P 21 21 21	P 21 21 21
Unit cell	47.3 77.0 137.3 90 90 90	46.6 77.3 137.0 90 90 90
Total reflections	166182 8456)	344821 (50985)
Unique reflections	19008 (962)	24768 (3925)
Multiplicity	8.7 (8.7)	13.9 (13.0)
Completeness (%)	99.8 (99.2)	99.7 (98.0)
Mean I/sigma(I)	11.2 (2.2)	19.4 (3.5)
Wilson B-factor	42.1	52.6
R-merge	0.094 (1.12)	0.118 (0.929)
R-pim	0.033 (0.382)	0.043 (0.316)
CC1/2	0.998 (0.872)	1.00 (0.940)
Anomalous correlation > 30%	N/A	45-3.4 Å
R-work	0.271 (0.362)	N/A
R-free	0.305 (0.435)	N/A
Number of non-hydrogen atoms	3137	N/A
Number of macromolecular atoms	3003	N/A
ligands		N/A
water	368	N/A

Protein residues	381	N/A
RMS(bonds) / Å	0.003	N/A
RMS(angles)/ °	0.64	N/A
Ramachandran favored (%)	99.7	N/A
Ramachandran outliers (%)	0	N/A
Clashscore	3.8	N/A
Average B-factor (Å^2)	79.70	N/A
macromolecules	79.90	N/A
ligands	0	N/A
solvent	75.10	N/A

Statistics for the highest-resolution shell are shown in parentheses.